Three Algorithms to Transform Displacement of the Proof-mass into Voltage Signals in a Simplicial Biaxial Accelerometer

TR-CIM-03-13 March, 2013

Xiaowei Shan, Jorge Angeles and James Richard Forbes

Centre for Intelligent Machines, Department of Mechanical Engineering
McGill University, Montréal, Canada

Abstract

In this paper we report the optimum pose estimation using a simplicial biaxial accelerometer (SBA). The estimation of the SBA proof-mass pose based on potentiometer measurements is discussed. Three different estimation algorithms are developed based on the kinematics of the proof-mass, while considering the impact of sensor noise. Numerical simulations are performed for the worst case scenario to demonstrate the effectiveness of the estimation algorithms, and Monte Carlo simulations provide a comprehensive evaluation of the algorithms under noise.

Keywords: accelerometer; proof-mass pose estimation; linear potentiometer

1 Introduction

The Simplicial-Biaxial-Accelerometer[1] [1] (SBA) is a novel realization of a biaxial accelerometer design [2]. The SBA is mounted rigidly on a rigid moving body under probing, which produces a motion of the proof-mass. The resulting relative displacement of the proof-mass with respect to the SBA frame produces an electronic signal, which obeys a relationship with the acceleration of the moving body [3]. Within the realm of Parallel-Kinematics Machines (PKM), the SBA proof-mass is suspended by three limbs, to produce two acceleration components to be measured by the SBA. Apparently, with one extra leg, the SBA provides redundancy in measurement, thereby increasing the precision and reducing measurement errors [2].

MEMS (Microelectromechanical Systems) technology realizes micro-scaled and accurate fabrication of the SBA, thus extending its applications significantly. However, several inevitable drawbacks accompany the MEMS fabrication, such as time-consumption and financially expensiveness [4]. Alternatively, the rapid prototype fabrication of the SBA is worth to be investigated, within the explosive development of 3D printers. The rapid prototype fabrication has its inherent advantages over other modeling approaches [5]. First of all, the overall fabrication process is apparently simplified and the time cost is reduced significantly. Moreover, the financial cost of rapid prototype is relatively much less expensive then the MEMS fabrication. In addition, rapid prototype is dominant over MEMS fabrication in fabricating complicated 3D architectures.

In this paper, three potentiometers are designed to attach to the vertices of the SBA proof-mass, to provide an electronic signal, for the purpose of rendering acceleration information of the proof-mass. However, the signal provided by the potentiometers denotes the relative displacement of its moving measurement shaft with respect to the housing, the displacement of the proof-mass is still unknown. Therefore, a study of the relationship of the proof-mass displacement with the displacement of each potentiometer becomes important. The relationship is investigated in details and the estimation algorithm is provided. Afterwards, a simulation example is studied to validate the algorithm, in order to obtain the range of estimation errors for the SBA. Finally, conclusions are offered.

2 Estimation Algorithms

The SBA is isotropic and without out-of-plane displacement; therefore, the motion of the proof-mass is considered as a coordinate transformation [6] in the frame plane with an origin shift $\boldsymbol{u}$ and a rotation defined by the rotation matrix $\boldsymbol{Q}(\theta)$ in terms of the angle θ, as shown in Fig. 2. Let a and s be the side length of the proof-mass and the frame, respectively, $d_i = \|\boldsymbol{q}_i - \boldsymbol{r}_i\|\,,\ i = 1, 2, 3$, the displacement measured by the ith potentiometer, and $\boldsymbol{p}_i,\ \boldsymbol{q}_i,\ \boldsymbol{r}_i$ the position vectors of $P_i,\ Q_i,\ R_i$, respectively.

The pose to be estimated comprises the translation $\boldsymbol{u}$ and the angle θ, which is, by design, a parasitic rotation of the order of 10^{-2} (rad) because of the stiffness of the Π-joints [7] that connect proof-mass to the frame.

[1]The term derives from *simplex*, a polyhedron with the minimum number of vertices embedded in $\mathbb{R}^n$.

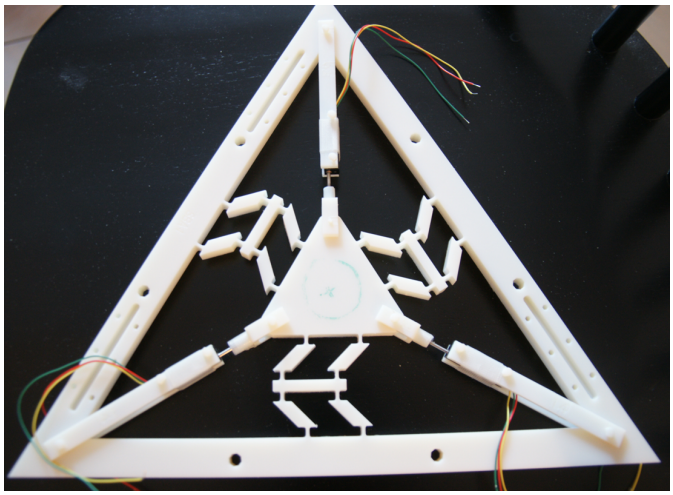

Figure 1: Physical prototype of the SBA

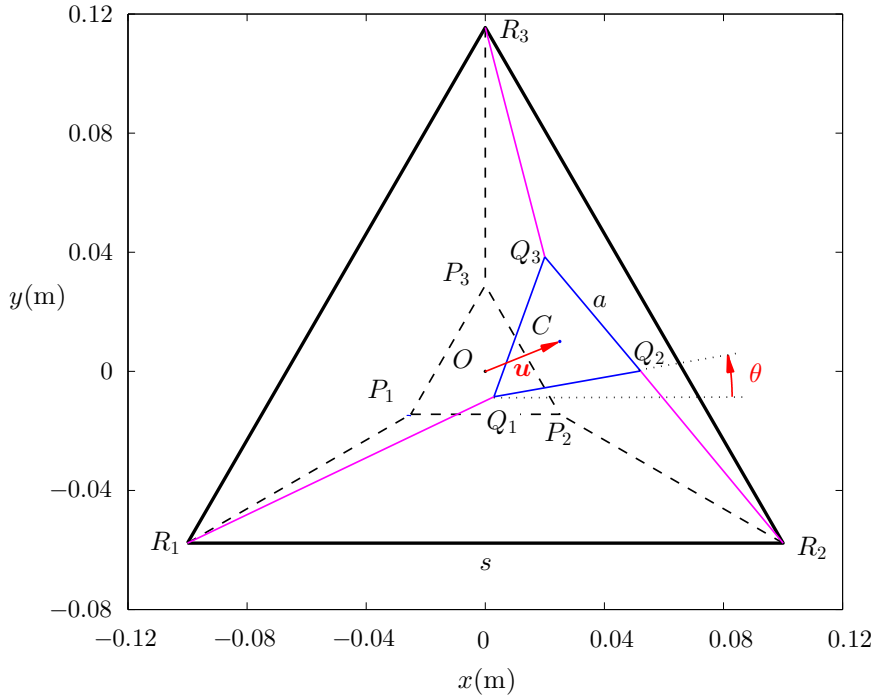

Figure 2: Schematic diagram of the prototype with potentiometers

In this paper, mainly three algorithms are devised and analyzed, which can be categorized according to the assumption of small rotation and the assembling position of the potentiometers.

- Algorithm 1: under the assumption of pure translation, and with the potentiometers pinned at the vertices of the proof-mass;
- Algorithm 2: under the assumption of pure translation, and with the potentiometers pinned at the centre of the proof-mass;
- Algorithm 3: under the assumption of both translation and rotation, and with the potentiometers pinned at the vertices of the proof-mass.

When evaluating the algorithms, the nonlinearity of the potentiometer η and the magnitude of the angle of rotation θ need to be considered at the same time to optimize the estimation of the translation of the proof-mass centre.

2.1 Algorithm 1

First, three equations can be obtained from the potentiometer readouts that constrain the vertices of the proof-mass onto the circles centred at the vertices of the frame.

$$\|\boldsymbol{q}_i - \boldsymbol{r}_i\| = d_i,\ i = 1, 2, 3 \tag{1}$$

Since the proof-mass is a rigid body and its motion is assumed to be a pure translation, the displacement of the vertices are identical with the displacement of the centre. Thus, the position vector of the vertices is $\boldsymbol{q}_i = \boldsymbol{u} + \boldsymbol{p}_i,\ i = 1, 2, 3$. Substituting these expressions into Eq. (1) and denoting $\boldsymbol{h}_i = \boldsymbol{p}_i - \boldsymbol{r}_i$ gives

$$\|\boldsymbol{u}\|^2 + 2\boldsymbol{h}_i^{\mathrm{T}}\boldsymbol{u} + \|\boldsymbol{h}_i\|^2 - d_i^2 = 0,\ i = 1, 2, 3 \tag{2}$$

Upon subtracting the above equations pairwise in Eq. (2), one obtains

$$2(\boldsymbol{h}_1 - \boldsymbol{h}_2)^{\mathrm{T}}\boldsymbol{u} = d_1^2 - d_2^2 \tag{3a}$$
$$2(\boldsymbol{h}_2 - \boldsymbol{h}_3)^{\mathrm{T}}\boldsymbol{u} = d_2^2 - d_3^2 \tag{3b}$$
$$2(\boldsymbol{h}_3 - \boldsymbol{h}_1)^{\mathrm{T}}\boldsymbol{u} = d_3^2 - d_1^2 \tag{3c}$$

Note that due to the assumption of pure translation, the three measurements are not independent; thus, two equations of the system determine the translation of the proof-mass. Upon considering all the useful information of the three equations, we end up with an overdetermined system of three equations with two unknowns, of the form

$$\boldsymbol{H}_1\boldsymbol{u} = \boldsymbol{\delta}_1 \tag{4}$$

where $\boldsymbol{H}_1$ and $\boldsymbol{\delta}_1$ are given by

$$\boldsymbol{H}_1 = \begin{bmatrix} 2(\boldsymbol{h}_1 - \boldsymbol{h}_2)^{\mathrm{T}} \\ 2(\boldsymbol{h}_2 - \boldsymbol{h}_3)^{\mathrm{T}} \\ 2(\boldsymbol{h}_3 - \boldsymbol{h}_1)^{\mathrm{T}} \end{bmatrix}, \quad \boldsymbol{\delta}_1 = \begin{bmatrix} d_1^2 - d_2^2 \\ d_2^2 - d_3^2 \\ d_3^2 - d_1^2 \end{bmatrix}.$$

whence an explicit expression of the displacement of the proof-mass is found using the Left Moore-Penrose Generalized Inverse (LMPGI)

$$\boldsymbol{u} = (\boldsymbol{H}_1^{\mathrm{T}}\boldsymbol{H}_1)^{-1}\boldsymbol{H}_1^{\mathrm{T}}\boldsymbol{\delta}_1 \tag{5}$$

Instead of computing the generalized inverse numerically, we will pursue a symbolic computation of the solution. The LMPGI is simplified with $\boldsymbol{h}_1 - \boldsymbol{h}_2 = (s-a)\boldsymbol{\iota}_2$, $\boldsymbol{h}_2 - \boldsymbol{h}_3 = (s-a)\boldsymbol{\iota}_3$, $\boldsymbol{h}_3 - \boldsymbol{h}_1 = (s-a)\boldsymbol{\iota}_1$, which yields

$$(\boldsymbol{H}_1^{\mathrm{T}}\boldsymbol{H}_1)^{-1}\boldsymbol{H}_1^{\mathrm{T}} = \frac{1}{3(s-a)} \begin{bmatrix} \boldsymbol{\iota}_2 & \boldsymbol{\iota}_3 & \boldsymbol{\iota}_1 \end{bmatrix}$$

Therefore Eq. (5) becomes

$$\begin{aligned} \boldsymbol{u} &= \frac{1}{3(s-a)}\big(\boldsymbol{\iota}_2(d_1^2 - d_2^2) + \boldsymbol{\iota}_3(d_2^2 - d_3^2) + \boldsymbol{\iota}_1(d_3^2 - d_1^2)\big) \\ &= \frac{\sqrt{3}}{6(s-a)} \begin{bmatrix} \sqrt{3}(d_1^2 - d_2^2) \\ d_1^2 + d_2^2 - 2d_3^2 \end{bmatrix} \end{aligned} \tag{6}$$

All the readouts of the potentiometer are reflected in Eq. (6) to provide a unique solution of the pose. Essentially, this algorithm filters the sensor noise unpon subtraction.

2.2 Geometric Interpretation of Algorithm 1

Since the three measurements from the potentiometers are not independent under the assumption of pure translation, only two measurements can determine the pose of the proof-mass, i.e., each pair of potentiometers and the corresponding side of the proof-mass can be regarded as a four-bar linkage, which leads to two possible poses for each pair of measurements out of three. As shown in Fig. 3, the dashed and solid segments symmetric about one side of the frame correspond to the two possible poses, but by construction, the proof-mass cannot move outside the frame; hence, one unique solution feasible for each pair of measurements is available.

If we characterise the pose estimated from a pair of measurements by a side of the proof-mass, when the measurement is disturbed by the sensor noise, we will have three links distributed asymmetrically, as shown in Fig. 3. Each intersection of the bisectors of a pair of segments yields an estimation of the centre of the proof-mass; therefore, by averaging the three intersections, an optimum estimation of the displacement of the proof-mass is obtained.

In Fig. 3, each end-point of the segments of the side-links is subscripted by first the original vertex number and then the segment number, the midpoint M_i of each segment $\mathcal{S}_i$, $i = 1, 2, 3$, is subscripted by the segment number, and a unit vector along each segment is defined by $\boldsymbol{\iota}_i$, $i = 1, 2, 3$. The actual centre position of the proof-mass is C, while the estimated one is denoted as C_{m}, the centroid of the intersections of the bisectors.

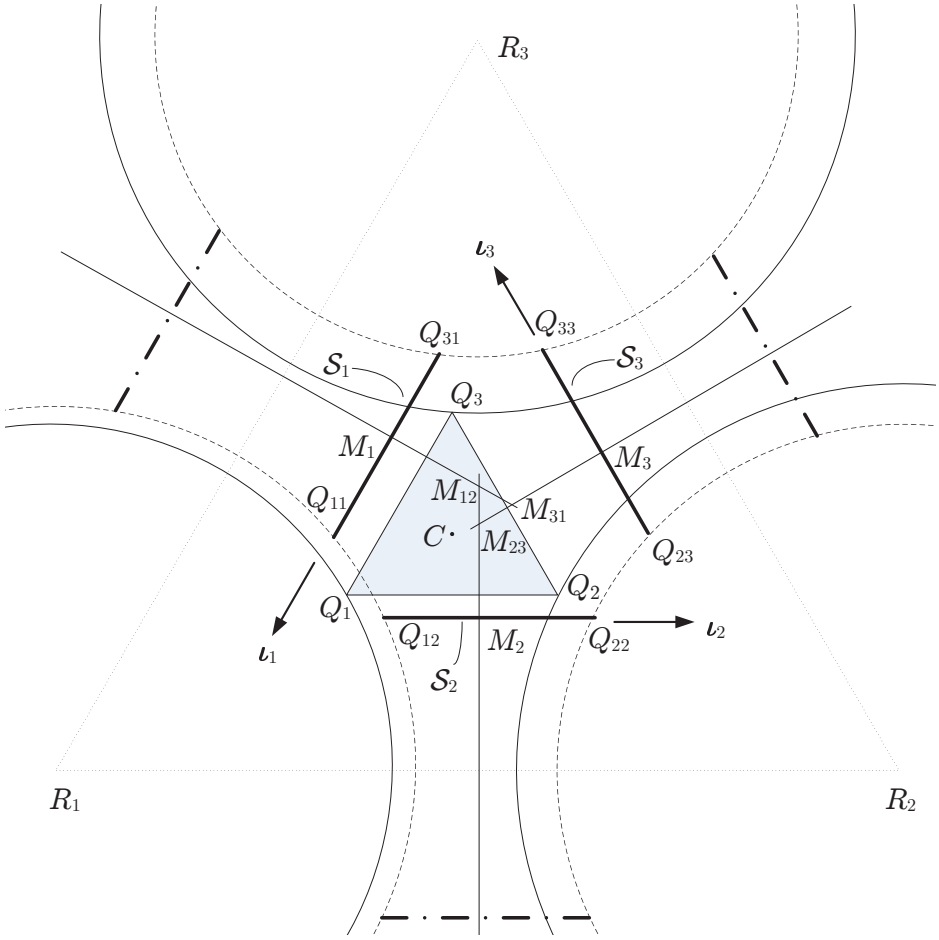

Figure 3: Asymmetric distribution of the side links

Similar to Eq. (1), each pair of potentiometers constrains one side of the proof-mass, and the end-points of segment $\mathcal{S}_i$ have the relations with the measurements shown in Eq. (7). Henceforth, index additions and subtractions are assumed to be mod (3). Without sensor noise, the three sides form a triangle, with the actual pose of the proof-mass; otherwise, the three sides will be distributed asymmetrically.

$$\|\boldsymbol{q}_{i-1,i} - \boldsymbol{r}_{i-1}\| = d_{i-1}, \quad \|\boldsymbol{q}_{i,i} - \boldsymbol{r}_i\| = d_i \tag{7}$$

With the assumption of pure translation, the end-points of each segment can be expressed in terms of its mid-point as

$$\boldsymbol{q}_{i-1,i} = \boldsymbol{m}_i - \frac{a}{2}\boldsymbol{\iota}_i, \quad \boldsymbol{q}_{i,i} = \boldsymbol{m}_i + \frac{a}{2}\boldsymbol{\iota}_i \tag{8}$$

Substituting Eq. (8) into Eq. (7) provides us with the expression of the midpoint for segment $\mathcal{S}_i$.

$$\|\boldsymbol{m}_i + \boldsymbol{r}_{i-1,i}\|^2 - d_{i-1}^2 = 0, \quad \|\boldsymbol{m}_i + \boldsymbol{r}_{i,i}\|^2 - d_i^2 = 0 \tag{9}$$

where

$$\boldsymbol{r}_{i-1,i} = \frac{a}{2}\boldsymbol{\iota}_i - \boldsymbol{r}_{i-1}, \quad \boldsymbol{r}_{i,i} = -\frac{a}{2}\boldsymbol{\iota}_i - \boldsymbol{r}_i.$$

Upon expansion of Eq. (9) and substraction of the equations for the same segments, notice that $\boldsymbol{r}_{i-1,i} - \boldsymbol{r}_{i,i} = (s-a)\boldsymbol{\iota}_i$, we obtain a projection relation of the midpoints,namely,

$$\mathcal{S}_i: \quad \boldsymbol{\iota}_i^{\mathrm{T}}\boldsymbol{m}_i = \frac{d_{i-1}^2 - d_i^2 - \|\boldsymbol{r}_{i-1,i}\|^2 + \|\boldsymbol{r}_{i,i}\|^2}{2(s-a)} \tag{10}$$

Now we search for the expression of the intersections of the bisectors of the three segments. Let $\boldsymbol{m}_{i-1,i}$ be the position vector of the intersection of the bisector of segment $\mathcal{S}_{i-1}$ and segment $\mathcal{S}_i$, which has the perpendicular relation with the unit vectors of the segments as

$$\boldsymbol{\iota}_{i-1}^{\mathrm{T}}(\boldsymbol{m}_{i-1,i} - \boldsymbol{m}_{i-1}) = 0, \quad \boldsymbol{\iota}_i^{\mathrm{T}}(\boldsymbol{m}_{i-1,i} - \boldsymbol{m}_i) = 0 \tag{11}$$

Next, we rewrite Eq. (11) in a compact form and substitute Eq. (10) from it. Although there will be two possible positions for each segment, their bisector are the same; hence, an explicit expression of the intersections can be found. Substituting the simplification $\|\boldsymbol{r}_{i,i}\|^2 - \|\boldsymbol{r}_{i-1,i}\|^2 = sa$ derived from the geometric relation yields

$$\begin{bmatrix} \boldsymbol{\iota}_i^{\mathrm{T}} \\ \boldsymbol{\iota}_{i-1}^{\mathrm{T}} \end{bmatrix} \boldsymbol{m}_{i-1,i} = \frac{1}{2(s-a)} \begin{bmatrix} d_{i-1}^2 - d_i^2 + sa \\ d_i^2 - d_{i+1}^2 + sa \end{bmatrix} \tag{12}$$

whence,

$$\boldsymbol{m}_{i-1,i} = \frac{1}{2(s-a)\Delta_{i-1,i}} \boldsymbol{E} \begin{bmatrix} -\boldsymbol{\iota}_{i-1} & \boldsymbol{\iota}_i \end{bmatrix} \boldsymbol{\delta}_{i-1,i} \tag{13}$$

where

$$\boldsymbol{E}=\begin{bmatrix} 0 & -1 \\ 1 & 0 \end{bmatrix},\quad \boldsymbol{\delta}_{i-1,i}=\begin{bmatrix} d_{i-1}^2-d_i^2+sa \\ d_i^2-d_{i+1}^2+sa \end{bmatrix},$$
$$\Delta_{i-1,i}=\det\left(\begin{bmatrix} \boldsymbol{\iota}_i^{\mathrm{T}} \\ \boldsymbol{\iota}_{i-1}^{\mathrm{T}} \end{bmatrix}\right)=\boldsymbol{\iota}_{i-1}^{\mathrm{T}}\boldsymbol{E}\boldsymbol{\iota}_i=-\cos 30^\circ=-\sqrt{3}/2$$

We choose the mean value of position vectors of the three intersections as the estimation of the displacement $\boldsymbol{u}_{\mathrm{m}}$ of the proof-mass, which yields

$$\begin{aligned}
\boldsymbol{u}_{\mathrm{m}}=&\frac{\boldsymbol{m}_{31}+\boldsymbol{m}_{12}+\boldsymbol{m}_{23}}{3}\\
=&\frac{1}{3}\sum_{i=1}^{3}\left(-\frac{\sqrt{3}}{3(s-a)}\boldsymbol{E}\begin{bmatrix} -\boldsymbol{\iota}_{i-1} & \boldsymbol{\iota}_i \end{bmatrix}\begin{bmatrix} d_{i-1}^2-d_i^2+sa \\ d_i^2-d_{i+1}^2+sa \end{bmatrix}\right)\\
=&-\frac{\sqrt{3}}{9(s-a)}\boldsymbol{E}\Bigg(\begin{bmatrix} -\boldsymbol{\iota}_3 & \boldsymbol{\iota}_1 \end{bmatrix}\begin{bmatrix} d_3^2-d_1^2 \\ d_2^2-d_3^2 \end{bmatrix}+(\boldsymbol{\iota}_1-\boldsymbol{\iota}_3)sa\\
&+\begin{bmatrix} -\boldsymbol{\iota}_1 & \boldsymbol{\iota}_2 \end{bmatrix}\begin{bmatrix} d_1^2-d_2^2 \\ d_3^2-d_1^2 \end{bmatrix}+(\boldsymbol{\iota}_2-\boldsymbol{\iota}_1)sa\\
&+\begin{bmatrix} -\boldsymbol{\iota}_3 & \boldsymbol{\iota}_2 \end{bmatrix}\begin{bmatrix} d_2^2-d_3^2 \\ d_1^2-d_2^2 \end{bmatrix}+(\boldsymbol{\iota}_3-\boldsymbol{\iota}_2)sa\Bigg)\\
=&-\frac{\sqrt{3}}{9(s-a)}\boldsymbol{E}\Bigg(\begin{bmatrix} -\boldsymbol{\iota}_3 & \boldsymbol{\iota}_1 \end{bmatrix}\begin{bmatrix} d_3^2-d_1^2 \\ d_2^2-d_3^2 \end{bmatrix}\\
&+\begin{bmatrix} -\boldsymbol{\iota}_1 & \boldsymbol{\iota}_2 \end{bmatrix}\begin{bmatrix} d_1^2-d_2^2 \\ d_3^2-d_1^2 \end{bmatrix}+\begin{bmatrix} -\boldsymbol{\iota}_2 & \boldsymbol{\iota}_3 \end{bmatrix}\begin{bmatrix} d_2^2-d_3^2 \\ d_1^2-d_2^2 \end{bmatrix}\Bigg)
\end{aligned}\tag{14}$$

Upon realizing that the three components in the brackets in Eq. (14) are equivalent, we obtain a brief expression of the displacement $\boldsymbol{u}_{\mathrm{m}}$ as

$$\boldsymbol{u}_{\mathrm{m}}=-\frac{\sqrt{3}}{6(s-a)}\begin{bmatrix} \sqrt{3}(d_2^2-d_1^2) \\ 2d_3^2-d_1^2-d_2^2 \end{bmatrix}\tag{15}$$

which is identical to Eq. (6) and, hence, verifies that the geometric interpretation of Algorithm 1 under noise is exactly as depicted in Fig. 3.

2.3 Algorithm 2

If the potentiometers are pinned at the centre of the proof-mass, the angle of rotation will not affect the measurement of the potentiometers, i.e., the proof-mass with any angle of rotation has the same displacement at the centre. Hence, Algorithm 1 is modified for the configuration of the potentiometers pinned at the centre of the proof-mass, which is denoted as Algorithm 2.

Since the potentiometers are directly connected to the centre of the proof-mass, $\boldsymbol{p}_i=0,\ i=1,2,3$ and Eq. (1) becomes

$$\|\boldsymbol{u}_{\mathrm{c}}-\boldsymbol{r}_i\|=d_i,\ i=1,2,3\tag{16}$$

about the displacement of the centre of the proof-mass $\boldsymbol{u}_\mathrm{c}$ for the centre-pinned configuration. Whence

$$\|\boldsymbol{u}_\mathrm{c}\|^2 - 2\boldsymbol{r}_i^\mathrm{T}\boldsymbol{u}_\mathrm{c} + \|\boldsymbol{r}_i\|^2 - d_i^2 = 0,\ i = 1, 2, 3 \tag{17}$$

Upon subtracting the above equations pairwise in Eq. (17), one obtains

$$2(\boldsymbol{r}_2 - \boldsymbol{r}_1)^\mathrm{T}\boldsymbol{u}_\mathrm{c} = d_1^2 - d_2^2 \tag{18a}$$
$$2(\boldsymbol{r}_3 - \boldsymbol{r}_2)^\mathrm{T}\boldsymbol{u}_\mathrm{c} = d_2^2 - d_3^2 \tag{18b}$$
$$2(\boldsymbol{r}_1 - \boldsymbol{r}_3)^\mathrm{T}\boldsymbol{u}_\mathrm{c} = d_3^2 - d_1^2 \tag{18c}$$

Similarly to Algorithm 1,

$$\boldsymbol{u}_\mathrm{c} = (\boldsymbol{H}_2^\mathrm{T}\boldsymbol{H}_2)^{-1}\boldsymbol{H}_2^\mathrm{T}\boldsymbol{\delta}_2 \tag{19}$$

where

$$\boldsymbol{H}_2 = \begin{bmatrix} 2(\boldsymbol{r}_2 - \boldsymbol{r}_1)^\mathrm{T} \\ 2(\boldsymbol{r}_3 - \boldsymbol{r}_2)^\mathrm{T} \\ 2(\boldsymbol{r}_1 - \boldsymbol{r}_3)^\mathrm{T} \end{bmatrix}, \quad \boldsymbol{\delta}_2 = \boldsymbol{\delta}_1 = \begin{bmatrix} d_1^2 - d_2^2 \\ d_2^2 - d_3^2 \\ d_3^2 - d_1^2 \end{bmatrix}.$$

the LMPGI in Eq. (19) is simplified with $\boldsymbol{r}_2 - \boldsymbol{r}_1 = s\boldsymbol{\iota}_2,\ \boldsymbol{r}_3 - \boldsymbol{r}_2 = s\boldsymbol{\iota}_3,\ \boldsymbol{r}_1 - \boldsymbol{r}_3 = s\boldsymbol{\iota}_1$

$$(\boldsymbol{H}_2^\mathrm{T}\boldsymbol{H}_2)^{-1}\boldsymbol{H}_2^\mathrm{T} = \frac{1}{3s}\begin{bmatrix} \boldsymbol{\iota}_2 & \boldsymbol{\iota}_3 & \boldsymbol{\iota}_1 \end{bmatrix}$$

which results in a simple expression for the estimation of the centre of the proof-mass

$$\boldsymbol{u}_\mathrm{c} = \frac{\sqrt{3}}{6s}\begin{bmatrix} \sqrt{3}(d_1^2 - d_2^2) \\ d_1^2 + d_2^2 - 2d_3^2 \end{bmatrix} \tag{20}$$

It can be seen that the only difference between Eq. (20) and Eq. (6) is the denominator, but the readouts $d_i,\ i = 1, 2, 3$ in Eq. (20) are not affected by the angle of rotation and, therefore, help to produce better estimation result.

2.4 Algorithm 3

Algorithm 3 aims at the estimation of the proof-mass pose, i.e., the translation and the angle of rotation of the proof-mass, simultaneously, with three unknowns in three equations derived from the constraints that the vertices of the proof-mass stay onto the circles defined by the potentiometers. In fact, the SBA with the three potentiometers, making abstraction of the ΠΠ limbs, has the architecture of a parallel robot with three RPR limbs and, hence, admits six forward kinematics solutions [8, 9]. However, considering the small-angle assumption of the rotation of the proof-mass and the range of the displacement constrained by the frame, we will have less than six feasible solutions for the pose of the proof-mass.

Upon augmenting Eq. (1), the corresponding expression in terms of the displacement $\boldsymbol{u}_\mathrm{r}$ and the angle of rotation θ of the proof-mass becomes

$$\|\boldsymbol{Q}(\boldsymbol{u}_\mathrm{r}+\boldsymbol{p}_i)-\boldsymbol{r}_i\| = d_i,\ i=1,2,3 \tag{21}$$

where

$$\boldsymbol{Q} = \begin{bmatrix} \cos(\theta) & -\sin(\theta) \\ \sin(\theta) & \cos(\theta) \end{bmatrix}, \quad \theta \in \left(-\frac{\pi}{2}, \frac{\pi}{2}\right)$$

Upon expansion, Eq. (21) leads to

$$\|\boldsymbol{u}_\mathrm{r}\|^2 + 2\boldsymbol{p}_i^\mathrm{T}\boldsymbol{Q}^\mathrm{T}\boldsymbol{u}_\mathrm{r} - 2\boldsymbol{r}_i^\mathrm{T}\boldsymbol{u}_\mathrm{r} + \|\boldsymbol{p}_i\|^2 - 2\boldsymbol{p}_i^\mathrm{T}\boldsymbol{Q}^\mathrm{T}\boldsymbol{r}_i + \|\boldsymbol{r}_i\|^2 - d_i^2 = 0,\ i=1,2,3 \tag{22}$$

As a result of the isotropy of the SBA, $\|\boldsymbol{p}_i\|$ and $\|\boldsymbol{r}_i\|$ can be denoted as p and r respectively, and $\sum_{i=1}^{3}\boldsymbol{p}_i = 0$, $\sum_{i=1}^{3}\boldsymbol{r}_i = 0$, $\boldsymbol{p}_i^\mathrm{T}\boldsymbol{Q}^\mathrm{T}\boldsymbol{r}_i = pr\cos\theta$. Then adding the equations for $i=1,2,3$ in Eq. (22) yields

$$\|\boldsymbol{u}_\mathrm{r}\|^2 = 2pr\cos\theta - p^2 - r^2 + \frac{d_1^2+d_2^2+d_3^2}{3} \tag{23}$$

Meanwhile, upon subtracting Eq. (22) pairwise, and expressing $\boldsymbol{r}_i = n\boldsymbol{p}_i,\ i=1,2,3$, and $\boldsymbol{Q} = \cos\theta\boldsymbol{I} + \sin\theta\boldsymbol{E}$, where $\boldsymbol{I}$ denotes the 2×2 identity matrix, one obtains

$$2\Big(\big((\cos\theta-n)\boldsymbol{I}-\sin\theta\boldsymbol{E}\big)\big(\boldsymbol{p}_1-\boldsymbol{p}_2\big)\Big)^\mathrm{T}\boldsymbol{u}_\mathrm{r} = d_1^2-d_2^2 \tag{24a}$$

$$2\Big(\big((\cos\theta-n)\boldsymbol{I}-\sin\theta\boldsymbol{E}\big)\big(\boldsymbol{p}_2-\boldsymbol{p}_3\big)\Big)^\mathrm{T}\boldsymbol{u}_\mathrm{r} = d_2^2-d_3^2 \tag{24b}$$

$$2\Big(\big((\cos\theta-n)\boldsymbol{I}-\sin\theta\boldsymbol{E}\big)\big(\boldsymbol{p}_3-\boldsymbol{p}_1\big)\Big)^\mathrm{T}\boldsymbol{u}_\mathrm{r} = d_3^2-d_1^2 \tag{24c}$$

among which, only two equations are independent; thus, we choose arbitrary two, say Eq. (24a) and Eq. (24b), which gives the expression of the displacement $\boldsymbol{u}_\mathrm{r}$ of the proof-mass with respect to the angle of rotation θ as follows

$$\boldsymbol{u}_\mathrm{r} = \frac{1}{2\Delta_3}\boldsymbol{E}\begin{bmatrix} -\boldsymbol{h}_{23} & \boldsymbol{h}_{12} \end{bmatrix}\boldsymbol{\delta}_3 \tag{25}$$

where

$$\begin{aligned}
\boldsymbol{h}_{12} &= \big((\cos\theta-n)\boldsymbol{I}-\sin\theta\boldsymbol{E}\big)\big(\boldsymbol{p}_1-\boldsymbol{p}_2\big) = -a\big((\cos\theta-n)\boldsymbol{I}-\sin\theta\boldsymbol{E}\big)\boldsymbol{\iota}_2,\\
\boldsymbol{h}_{23} &= \big((\cos\theta-n)\boldsymbol{I}-\sin\theta\boldsymbol{E}\big)\big(\boldsymbol{p}_2-\boldsymbol{p}_3\big) - a\big((\cos\theta-n)\boldsymbol{I}-\sin\theta\boldsymbol{E}\big)\boldsymbol{\iota}_3,\\
\Delta_3 &= \det\left(\begin{bmatrix} \boldsymbol{h}_{12}^\mathrm{T} \\ \boldsymbol{h}_{23}^\mathrm{T} \end{bmatrix}\right) = \boldsymbol{h}_{23}^\mathrm{T}\boldsymbol{E}\boldsymbol{h}_{12} = \frac{\sqrt{3}a^2}{2}\big(\sin^2\theta+(n-\cos\theta)^2\big)^2,\\
\boldsymbol{\delta}_3 &= \begin{bmatrix} d_1^2-d_2^2 \\ d_2^2-d_3^2 \end{bmatrix}
\end{aligned}$$

Hence, the simplified form of Eq. (25) is

$$\boldsymbol{u}_{\mathrm{r}} = \frac{\big(\sin\theta\boldsymbol{I} + (n-\cos\theta)\boldsymbol{E}\big)\begin{bmatrix} -\boldsymbol{\iota}_3 & \boldsymbol{\iota}_2 \end{bmatrix}\boldsymbol{\delta}_3}{\sqrt{3}a\big(\sin^2\theta + (n-\cos\theta)^2\big)} \tag{26}$$

We denote $\boldsymbol{Q}' = \sin\theta\boldsymbol{I} + (n-\cos\theta)\boldsymbol{E}$, which is not a rotation matrix, and $\boldsymbol{L} = \begin{bmatrix} -\boldsymbol{\iota}_3 & \boldsymbol{\iota}_2 \end{bmatrix}$. Then an alternative expression of $\|\boldsymbol{u}_{\mathrm{r}}\|^2$ is derived by manipulating Eq. (26), namely

$$\begin{aligned}
\|\boldsymbol{u}_{\mathrm{r}}\|^2 = \boldsymbol{u}_{\mathrm{r}}^{\mathrm{T}}\boldsymbol{u}_{\mathrm{r}} &= \frac{\boldsymbol{\delta}_3^{\mathrm{T}}\boldsymbol{L}^{\mathrm{T}}\boldsymbol{Q}'^{\mathrm{T}}\boldsymbol{Q}'\boldsymbol{L}\boldsymbol{\delta}_3}{3a^2\big(\sin^2\theta + (n-\cos\theta)^2\big)^2} \\
&= \frac{\boldsymbol{\delta}_3^{\mathrm{T}}\boldsymbol{L}^{\mathrm{T}}\big(\sin\theta\boldsymbol{I} - (n-\cos\theta)\boldsymbol{E}\big)\big(\sin\theta\boldsymbol{I} + (n-\cos\theta)\boldsymbol{E}\big)\boldsymbol{L}\boldsymbol{\delta}_3}{3a^2\big(\sin^2\theta + (n-\cos\theta)^2\big)^2} \\
&= \frac{\boldsymbol{\delta}_3^{\mathrm{T}}\boldsymbol{L}^{\mathrm{T}}\big(\sin^2\theta + (n-\cos\theta)^2\big)\boldsymbol{I}\boldsymbol{L}\boldsymbol{\delta}_3}{3a^2\big(\sin^2\theta + (n-\cos\theta)^2\big)^2} \\
&= \frac{\boldsymbol{\delta}_3^{\mathrm{T}}\boldsymbol{L}^{\mathrm{T}}\boldsymbol{L}\boldsymbol{\delta}_3}{3a^2\big(\sin^2\theta + (n-\cos\theta)^2\big)} \\
&= \frac{1}{3a^2(1+n^2-2n\cos\theta)}\boldsymbol{\delta}_3^{\mathrm{T}}\begin{bmatrix} \|\boldsymbol{\iota}_3\|^2 & -\boldsymbol{\iota}_3^{\mathrm{T}}\boldsymbol{\iota}_2 \\ -\boldsymbol{\iota}_3^{\mathrm{T}}\boldsymbol{\iota}_2 & \|\boldsymbol{\iota}_2\|^2 \end{bmatrix}\boldsymbol{\delta}_3 \\
&= \frac{1}{3a^2(1+n^2-2n\cos\theta)}\boldsymbol{\delta}_3^{\mathrm{T}}\begin{bmatrix} 1 & 1/2 \\ 1/2 & 1 \end{bmatrix}\boldsymbol{\delta}_3 \\
&= \frac{d_1^4 + d_2^4 + d_3^4 - d_1^2d_2^2 - d_2^2d_3^2 - d_1^2d_3^2}{3a^2(1+n^2-2n\cos\theta)}
\end{aligned} \tag{27}$$

From Eqs. (23) and (27), a quadratic equation in $\cos\theta$ is obtained with only the configuration parameters and the measurement of the potentiometers

$$4n^2a^4\cos^2\theta - 2na^2\big(2a^2(1+n^2) - d'\big)\cos\theta - a^2(1+n^2)d' + a^4(1+n^2)^2 + d'' = 0 \tag{28}$$

where

$$d' = d_1^2 + d_2^3 + d_3^2; \quad d'' = d_1^4 + d_2^4 + d_3^4 - d_1^2d_2^2 - d_2^2d_3^2 - d_3^2d_1^2$$

Upon substitution of the tan-half-angle identities

$$\cos\theta = \frac{1-\tau^2}{1+\tau^2}, \text{ where } \tau \equiv \tan^2\left(\frac{\theta}{2}\right)$$

and the configuration parameters $n = 4,\ a = 0.05$ (m) into Eq. (28), a quartic equation in τ is obtained, whose roots are

$$\tau_{1,2} = \pm\frac{\sqrt{2}}{10}\sqrt{-50 - \frac{32}{8(d_1^2+d_2^2+d_3^2) + 8\sqrt{3}\sqrt{2d_1^2d_2^2+2d_1^2d_3^2+2d_2^2d_3^2-d_1^4-d_2^4-d_3^4}-1}}$$
$$\tau_{3,4} = \pm\frac{1}{5}\sqrt{-25 - \frac{16}{8(d_1^2+d_2^2+d_3^2) - 8\sqrt{3}\sqrt{2d_1^2d_2^2+2d_1^2d_3^2+2d_2^2d_3^2-d_1^4-d_2^4-d_3^4}-1}} \tag{29}$$

among which, $\tau_{1,2}$ are real and feasible, while $\tau_{3,4}$ complex and can be discarded. Therefore, a pair of solutions with opposite signs is obtained for the angle of rotation θ, but only the actual value of the angle of rotation produces a proper estimation of the displacement of the proof-mass $\boldsymbol{u}_{\mathrm{r}}$ from Eq. (26).

Since the displacements calculated from the two feasible angles of rotation are not symmetric, a method for identifying the two solutions is needed, such as comparing with the estimation result from Algorithm 1 to eliminate one solution. In addition, when the system is disturbed by the sensor noise, $\tau_{1,2}$ sometimes becomes complex and gives no real solution. Yet, the valid results of the angle of rotation provide a rough estimation of the parasitic rotation occuring during the test.

3 Numerical Simulations

To obtain the range of the estimation errors, the worst case scenario of estimating the displacement of centre of the proof-mass during the prototype test is simulated in Matlab with Algorithm 1, 2 and 3 aforementioned. The comprehensive influence of the parasitic rotation and the nonlinearity of the potentiometers is shown for Algorithm 1 to estimate of the translation of the proof-mass. In addition, a set of 10000 trial runs of Monte Carlo simulation [10] is done to approximate the real test, which provides a comprehensive evaluation of the Algorithms.

3.1 Simulation Parameters

The designed trajectory of the proof-mass is: 50 positions of the centre of the proof-mass with its x, y coordinates both moving from $-3\sqrt{2}\times10^{-3}$ (m) to $3\sqrt{2}\times10^{-3}$ (m), resulting in a 45-degree segment of 12 (mm). In this case, the largest stretch of the potentiometers is 5.86 (mm), which is smaller than the limit of half the stroke 6 (mm) and covers the measurement range at best.

Since the parasitic rotation of the proof-mass is of the order of 10^{-2} (rad), it is assumed that the range of the angle of rotation is $[-10^{-2}, 10^{-2}]$. Meanwhile, according to the data sheet of the potentiometer LCP8T-12-10K, the independent nonlinearity of the sensor is $\pm2\%$. In order to interpret this information, we referred to Celesco's miniature MLP series linear potentiometers and take the nonlinearity for the full stroke, which is illustrated in Fig. 4(a) for an arbitrary angle of inclination ψ.

The LCP8T-12-10K potentiometer is electronically tested to be most reliable around the middle of the stroke, as shown in Fig. 4(b), where l represents the displacement of the core from its retracted position and V the output voltage of the potentiometer; therefore, we locate the home stretch of the potentiometers at 6 (mm), which also allows the proof-mass to move in both directions

along the potentiometers. In Fig. 4(a) at the full stroke 12 (mm) and 0 (mm), the measurement with its maximum nonlinearity is $(1 \pm 2\%)y_{\mathrm{p}}$ in the linear function $y_{\mathrm{p}} = \tan(\psi)x_{\mathrm{p}}$.

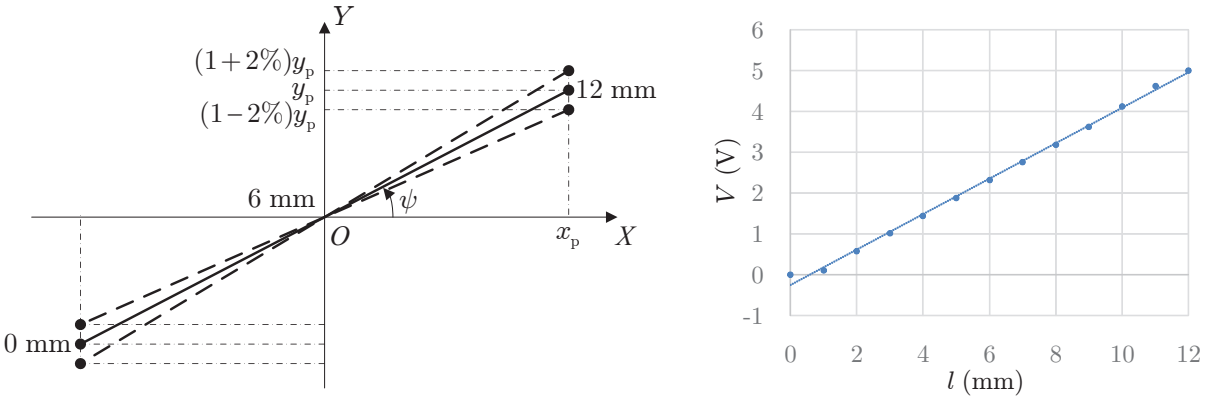

(a) Nonlinearity of the potentiometer in full stroke (b) Test of the nonlinearity of LCP8T-12-10K

Figure 4: Interpretation of the nonlinearity of the potentiometer

3.2 Analysis and Comparison of Simulation Results

For the worst case scenario of estimating the displacement of the centre of the proof-mass, four combinations of the sensor noise and the angle of rotation are simulated for the designed trajectory. Table 1 is a brief summary of the estimation errors with Algorithm 1, 2 and 3, where $\eta = \pm 2\%$ represents $\eta_1 = -2\%, \eta_2 = 2\%, \eta_3 = -2\%$ for the three potentiometers to avoid identical values of the nonlinearity. Besides, Fig. 5, corresponding to Table 1, shows the estimation error $\boldsymbol{\epsilon}$ of the position vectors of the centre of the proof-mass along the designed trajectory.

Simplified Eq. (6) and Eq. (20) are used for Algorithm 1 and Algorithm 2 respectively, while the estimation with Algorithm 3 is obtained from Eq. (26) and Eq. (29). Sometimes, the sensor noise causes the estimation of the angle of rotation to be complex, which is compromised by taking the asbolute value of the angle, and then producing the estimation of the translation of the proof-mass.

Table 1: Estimation errors of the centre of the proof-mass (m)

Conditions	Value type	Algorithm 1	Algorithm 2	Algorithm 3
a) $\eta = 0$	mean	8.1730×10^{-18}	1.0380×10^{-17}	9.4082×10^{-12}
$\theta = 0$ (rad)	max.	2.1290×10^{-17}	2.7706×10^{-17}	5.2684×10^{-11}
b) $\eta = 0$	mean	1.0204×10^{-5}	1.0380×10^{-17}	1.2939×10^{-17}
$\theta = 1 \times 10^{-2}$ (rad)	max.	2.0000×10^{-5}	2.7706×10^{-17}	3.9474×10^{-17}
c) $\eta = \pm 2\%$	mean	2.9732×10^{-5}	2.9712×10^{-5}	2.9308×10^{-5}
$\theta = 0$ (rad)	max.	5.8537×10^{-5}	5.8418×10^{-5}	6.0971×10^{-5}
d) $\eta = \pm 2\%$	mean	3.4646×10^{-5}	2.9712×10^{-5}	2.8237×10^{-5}
$\theta = 1 \times 10^{-2}$ (rad)	max.	6.8892×10^{-5}	5.8418×10^{-5}	5.6560×10^{-5}

Without disturbance of the sensor noise and the parasitic rotation, it can be seen from Table 1 that every devised algorithm has accurate estimation of the position of the centre of the proof-mass; while under the disturbance of the sensor noise and the parasitic rotation, the magnitude of the estimation errors are all suppressed to the order lower than 10^{-5}, i.e. 2 orders lower than the magnitude of the displacement of the proof-mass, even in the worst case scenario at the bottom line.

Generally speaking, Algorithm 2 for the centre-pinned configuration is the most accurate in all cases, however, this algorithm loses the chance to get the estimation of the angle of rotation, while Algorithm 3 has comparable results with Algorithm 2 and provides us a glimpse of the magnitude of the angle of rotation as shown in Table 2.

Table 2: Estimation errors of the angle of rotation with Algorithm 3 (rad)

Conditions	a) $\eta = 0$ $\theta = 0$ (rad)	b) $\eta = 0$ $\theta = 1 \times 10^{-2}$ (rad)	c) $\eta = \pm 2\%$ $\theta = 0$ (rad)	d) $\eta = \pm 2\%$ $\theta = 1 \times 10^{-2}$ (rad)
mean	1.0457×10^{-8}	9.3089×10^{-15}	1.5572×10^{-2}	6.9685×10^{-3}
max.	2.6342×10^{-8}	3.6138×10^{-14}	2.5435×10^{-2}	1.3246×10^{-2}

Comparing the estimation errors in Condition b) and c), we can conclude that the impact of the nonlinearity of the potentiometer is larger than the parasitic rotation of the proof-mass, which is further proved in Fig. 6 for the extreme position $(3\sqrt{2} \times 10^{-3}, 3\sqrt{2} \times 10^{-3})$ (m) of the centre of the proof-mass. The magnitude of the estimation error ϵ depends on the integrative impact of disturbances, and is larger along the direction of the nonlinearity η than along the direction of the parasitic angle θ in Fig. 6. Even if the sensor noise has the same range as the angle of rotation, e.g. $[-0.01, 0.01]$, the projection of the ϵ-surface onto the θ-η plane shows that the extreme values ± 0.01 of θ coincide with the tangent to the curve of cooler colour than η, indicating that the sensor noise is the major source of the estimation error.

Comparing the performance of Algorithm 1 and Algorithm 3 in Condition b), c) and d), it is shown that Algorithm 3 has slightly better estimation results of the translation of the proof-mass; although it is shown in Table 2 that Algorithm 3 does not have a high accuracy of the angle of rotation, the superiority of Algorithm 3 is basically the distraction of the sensor noise to partially upon the rotation of the proof-mass, thus resulting in a better estimation of the translation. This is also why Algorithm 3 has even higher accuracy than Algorithm 2 under Condition c) and d).

It should be noticed that the worst case scenario for estimating the angle of rotation is not the same with estimating the displacement of the proof-mass. The former is under maximum sensor noise and small rotation, which can be seen from comparing condition c) and d) in Table 2. This implies that the comprehensive performance of the algorithms under random sensor noise and angle of rotation is not obvious for Algorithm 3 and needs to be further evaluated. To this end, a set of 10000×50 random combinations of the sensor noise and the angle of rotation is simulated for the 50 sample points of the centre of the proof-mass, in which the ranges of the sensor noise and the angle of rotation are $[-2 \times 10^{-2}, 2 \times 10^{-2}]$ and $[-1 \times 10^{-2}, 1 \times 10^{-2}]$ (rad), respectively.

Table 3 lists the mean value of the 10000 trial runs for the estimation of the displacement of the centre of the proof-mass, where the mean values and the maximum values refer to the

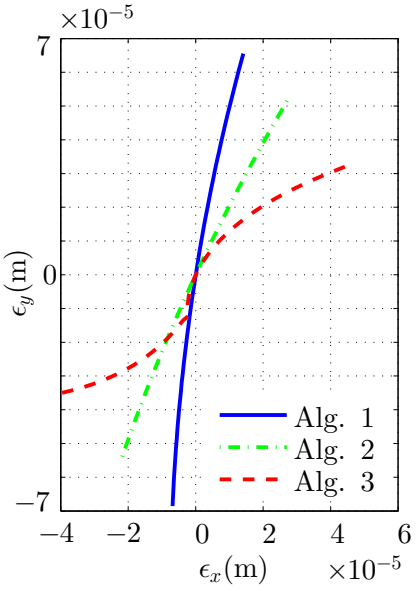

Figure 5: Estimation error $\boldsymbol{\epsilon}$

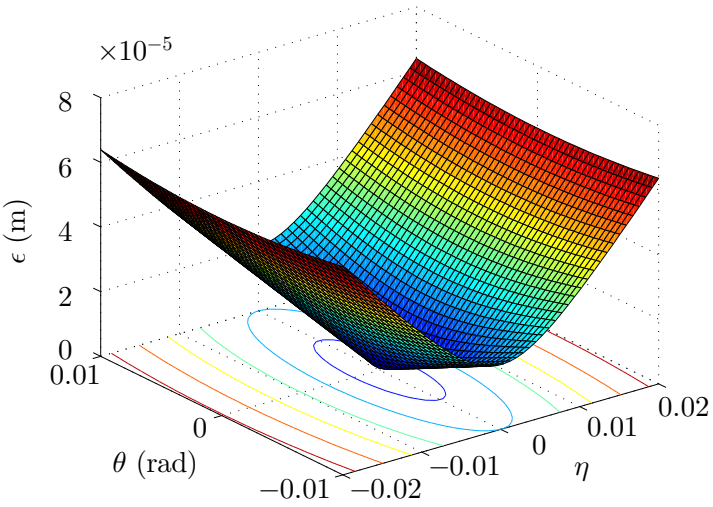

Figure 6: Magnitude of the estimation errors

estimation errors of the 50 sample points. It is shown that Algorithm 2 has the best performance comprehensively, while Algorithm 3 loses its superiority; Algorithm 1 has a comparable accuracy to Algorithm 2 and applies to the configuartion of the prototype for test, therefore sufficing the need of estimating the displacement of the centre of the proof-mass.

Table 3: Comprehensive estimation errors of the centre of the proof-mass (m)

Algorithm	Algorithm 1	Algorithm 2	Algorithm 3
mean value	1.5145×10^{-5}	1.3113×10^{-5}	2.0396×10^{-5}
maximum value	4.8874×10^{-5}	3.8857×10^{-5}	6.8525×10^{-5}

Moreover, the maximum value of the estimation error with Algorithm 3 is larger than any of the values with this algorithm under the typical conditions in Table 1, which evidence the intricate impact of the sensor noise and the angle of rotation to the estimation accuracy. On the other hand, the estimation of the angle of rotation with Algorithm 3 is found to be in the same order of magnitude as the nonlinearity of the potentiometer, since the angle of rotation is small and prone to sensor noise.

4 Conclusions

Simulation results validated the devised estimation algorithms. The impact of the nonlinearity of the potentiometers was suppressed to two orders of magnitude lower then the dimension of the translation of the proof-mass. Although numerically the potentiometer and the parastic angle of

rotation had the same order of uncertainty, the sensor noise was the main error source and needs to be considered during purchase of the potentiometers. The simulation results show that it is optimum to adopt Algorithm 1 under the assumption of pure translation. If better performance is desired or the angle of rotation is necessary, more potentiomters could be installed for Least-Square filtering.

References

[1] Kreyszig, E. *Advanced Engineering Mathematics*. John Wiley & Sons, New York, 1997.

[2] Zou, T. and Angeles, J. *Structural and Instrumentation Design of a MEMS Biaxial Accelerometer*. Technical Report TR-CIM-06-12, Department of Mechanical Engineering and Centre for Intelligent Machines, McGill University, Montreal, 2012.

[3] Cardou, P. and Angeles, J. "Simplectic architectures for true multi-axial accelerometers: a novel application of parallel robots." pp. 181–186. IEEE International Conference on Robotics and Automation, Rome, Italy, 2007.

[4] Cornelius, T. *MEMS/NEMS Handbook Techniques and Applications*. MEMS/NEMS Handbook Techniques and Applications, 2006.

[5] Yan, X. and Gu, P. "A review of rapid prototyping technologies and systems." *Computer-Aided Design*, Vol. 28, pp. 307–318, 1996.

[6] Angeles, J. *Fundamentals of Robotic Mechanical Systems: Theory, Methods, and Algorithms*. Third ed.. Springer, New York, NY, 2007.

[7] Cardou, P. and Angeles, J. "Simplectic Architectures for True Multi-axial Accelerometers: A Novel Application of Parallel Robots." *Proc. of the IEEE International Conference on Robotics and Automation, Rome, April 10-14, 2007*.

[8] Gosselin, C.M., Sefrioui, J. and Richard, M.J. "Solutions polynomiales au probléme de la cinèmatique directe des manipulateurs paralléles plans á trois degrès de libertè.", 1992.

[9] Merlet, J.P. *Parallel Robots*. Springer, Dordrecht, The Netherlands, 2006.

[10] Crassidis, J.L. and Junkins, J.L. *Optimal Estimation of Dynamic Systems*. Second ed.. CRC Press, Taylor and Francis Group, Boca Raton, FL, 2012.